HHS Public Access

Author manuscript

Bioconjug Chem. Author manuscript; available in PMC 2021 December 28.

Published in final edited form as:

Bioconjug Chem. 2015 December 16; 26(12): 2435–2441. doi:10.1021/acs.bioconjchem.5b00490.

Labeling Monomeric Insulin with Renal-Clearable Luminescent Gold Nanoparticles

Rodrigo D. Vinluan III, **Mengxiao Yu**, **Melissa Gannaway**, **Justin Sullins**, **Jing Xu**, **Jie Zheng**[*]

Department of Chemistry, The University of Texas at Dallas, Richardson, Texas 75080, United States

Abstract

In the native physiological environment, inorganic nanoparticles (NPs) often induce nonspecific protein adsorption, which could significantly alter the function of the proteins they labeled. As a result, small fluorescent dyes are still widely used in the imaging of proteins in animals due to their minimal interference with protein function. Here, we used monomeric insulin as a model and compared its bioactivity before and after labeling with renal-clearable near-infrared-emitting gold NPs. These NPs were chosen because they have high resistance to serum protein adsorption and low nonspecific accumulation. We have found that a 1:1 insulin–NP ratio can be achieved, where the insulin–NPs show minimal serum protein binding with fully retained bioactivity comparable to that of unlabeled insulin. These results show a proof of concept that renal-clearable NPs can behave like small molecules in protein labeling without changing the individual protein's function, laying down a foundation for in vivo tracking of proteins with multimodality imaging techniques.

Graphical Abstract

[*]**Corresponding Author**: jiezheng@utdallas.edu.

Supporting Information

The Supporting Information is available free of charge on the ACS Publications website at DOI: 10.1021/acs.bioconjchem.5b00490. ICP-MS results of the GS-AuNPs, ELISA studies, HR-TEM images, DLS data, absorption spectra, description of HPLC conditions, BGL studies of Cy5.5-insulin and pure GS-AuNPs, and renal clearance kinetics studies (PDF)

The authors declare no competing financial interest.

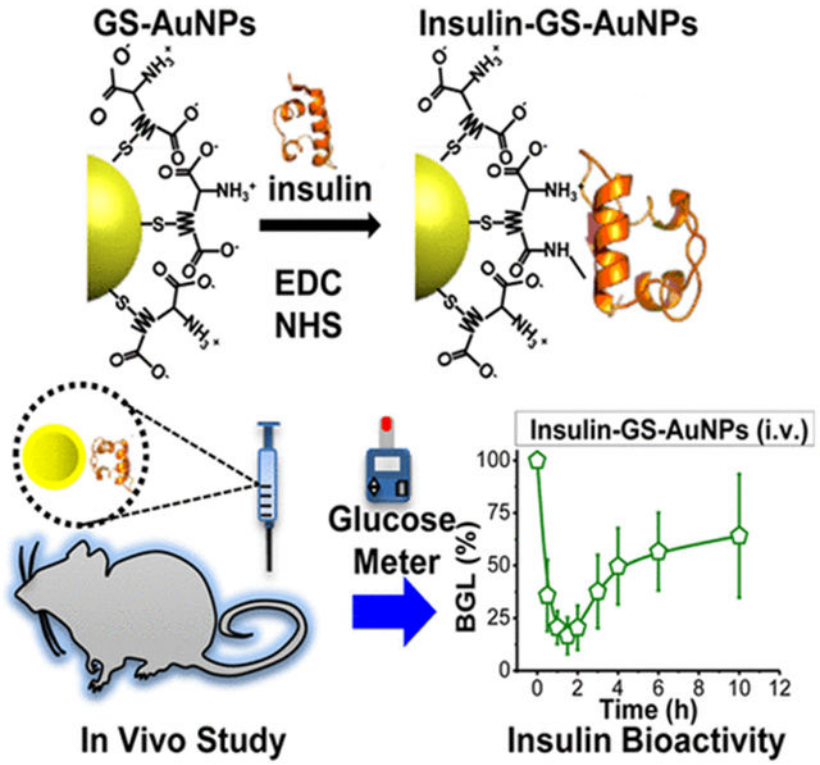

INTRODUCTION

Inorganic nanoparticles (NPs) with strong signal output and diverse material properties have been widely used as multimodality imaging contrast agents.[1–9] Although the conjugation of specific proteins to enhance the targeting delivery of inorganic NPs has been well demonstrated,[1–9] these NPs are not as widely used as small molecular probes[10] in the labeling of small proteins for in vivo imaging for a variety of reasons. First, due to the large surface areas of the NPs, multiple copies of proteins are often simultaneously coated onto the particle surface. As a result, the multivalency effect can occur,[11] a phenomenon known to induce distinct signaling pathways[12] and create biological concerns, because the cross-linking of surface proteins or the clustering of receptors is highly probable.[13] Second, the nonspecific adsorption of serum proteins on the NPs' surface while in the native physiological environment leads to the formation of protein corona, which restricts the functions of the proteins conjugated to the NPs, initiates nonspecific liver uptake, and alters the NPs' in vivo biodistributions and clearance pathways.[14] For instance, the biodistribution of ^{111}In-labeled bovine serum albumin (^{111}In-BSA) differs significantly compared to the BSA-conjugated gold nanoclusters (AuNC-BSA) with an average hydrodynamic diameter (HD) of ~7 nm, where only ~25%ID ^{111}In-BSA was found in the liver and kidney, while ~80%ID AuNC-BSA accumulated in the same organs.[15,16] Because of these challenges, labeling small proteins with small molecular contrast agents is still the most widely used technique for in vivo imaging, while the strengths of inorganic NPs in multimodality and protein labeling have not been fully appreciated.

The emergence of renal-clearable and multimodal inorganic NPs could open a new pathway to address this long-term challenge.[17–19] Unlike the conventional non-renal-clearable nanoprobes,[20–25] renal-clearable inorganic NPs can behave more like small molecules in terms of their rapid distribution into the body, evasion of liver uptake, and excretion through the urinary system.[26] In the past few years, renal-clearable NPs have been developed and used as contrast agents.[17–19,26,27] Furthermore, some of these NPs have luminescence in the NIR region,[19,28–30] which is suitable for in vivo fluorescence imaging due to the reduced autofluorescence that is inherent in many biomolecules. For example, NIR emitting glutathione-coated gold NPs (GS-AuNPs) have been shown to have the ability to passively target tumors and were utilized in the imaging of tumor-bearing mice in vivo via fluorescence imaging.[30] However, whether this new class of nanoprobes can be used in protein labeling is still unexplored. To answer this fundamental question, we used well-studied monomeric insulin as a model,[31] and labeled it with renal-clearable NIR emitting GS-AuNPs for several reasons. First, monomeric insulin is known to lower the glucose concentration in the blood, in which the insulin's bioactivity can be readily and accurately monitored by measuring the blood glucose level (BGL) of diabetic mice. Second, the monomeric insulin has an average HD of ~2.5 nm,[32] while the renal-clearable GS-AuNPs are ~3 nm, limiting the number of insulin molecules that can be attached to the surface of a single GS-AuNP. Third, renal-clearable GS-AuNPs with a core size of ~1.5 nm have a theoretical molecular mass of ~20 kDa (see Figure S1), much larger than that of insulin (~6 kDa, respectively). Fourth, although there have been a few reports regarding insulin-conjugated AuNPs in the past,[33–35] the NIR emission from renal-clearable GS-AuNPs would allow us to readily monitor the behaviors of insulin at the in vivo level. For instance, Bhumkar et al. demonstrated the use of plasmonic AuNPs as carriers for drug delivery and reported the transmucosal delivery of insulin loaded AuNPs.[33] These insulin loaded AuNPs were able to reduce the BGL of diabetic rats up to 30% 2 h after oral delivery, whereas the pure insulin showed very poor reduction due to their immediate degradation in the gastrointestinal tract. On the other hand, Liu et al. showed that 670-nm-emitting gold nanoclusters (AuNCs) can be synthesized directly using insulin. However, exactly how AuNCs were bound to insulin is not clear and hardly controlled.[35] In contrast, the results of our study show that monovalent labeling of insulin can be achieved with renal-clearable NIR-emitting GS-AuNPs. In addition, these insulin-GS-AuNPs have low affinity to serum proteins and can lower the blood glucose concentration of normal and diabetic mice, where the BGL dropped by ~80% of the initial value, which is comparable to the bioactivity of free insulin. Furthermore, we found that the untargeted insulin-GS-AuNPs are capable of renal clearance, and the changes in the biodistribution of these NPs were mainly governed by the protein–receptor interactions of the insulin ligand rather than the conjugates' overall HD. Hence, this work presents a proof of concept that renal-clearable NPs can behave like small molecules in protein labeling without changing the individual protein's function.

RESULTS AND DISCUSSION

NIR-emitting GS-AuNPs were synthesized according to a previously reported method via the thermal reduction of $AuCl_4^-$ (150 μL of 1 M $HAuCl_4$) by glutathione (5 mL 24 mM in 45 mL deionized H_2O) at 95 °C (Supporting Information (SI)).[28,29] To form the

insulin-GS-AuNPs, the amine group of insulin was conjugated to the carboxyl group of GS-AuNPs via the EDC-NHS coupling reaction (Figure 1A). The insulin-GS-AuNPs were purified extensively as described in a detailed procedure (SI). The IR spectra of the NPs and insulin are shown in Figure 1B. The IR spectrum of pure insulin reveals two signature peaks at ~1650 and ~1560 cm^{-1},[36] both of which are present in the spectrum of the insulin-GS-AuNPs but completely absent in the GS-AuNPs' spectrum. The average core diameter of insulin-GS-AuNPs was ~1.57 nm which is similar to that of the pure GS-AuNPs (~1.55 nm), based on the TEM analysis (Figure S2). Figure 1C reveals that the insulin-GS-AuNPs have an average HD of 5.9 ± 1.3 nm, roughly 2.7 nm larger than that of the unconjugated GS-AuNPs (3.2 ± 0.6 nm), as expected since monomeric insulin itself has an HD of ~2.5 nm.[32] The slight increase in the GS-AuNPs' average HD after insulin conjugation implies that the ratio of insulin molecules per NP is roughly 1 to 1, although some of the NPs may have multiple insulin molecules on their surface. In addition, the high-performance liquid chromatography (HPLC) data show that the insulin-GS-AuNPs have a shorter retention time (7.2 min) than the pure GS-AuNPs (8.1 min) as depicted in Figure 1D. This result also indicates the successful attachment of insulin on the NP surface.

To further confirm the insulin to GS-AuNP ratio, we used and combined the strengths of inductively coupled plasma mass spectrometry (ICP-MS) and enzyme linked immunosorbent assay (ELISA). These methods have allowed us to approximately quantify the total number of Au atoms and insulin molecules in the sample, as calculated and shown in Figure S1. For instance, the concentration of human insulin in the sample was determined to be 3.02 μg/mL via ELISA, as shown in Figure S1B. On the other hand, it has been shown that there are about 102 Au atoms in a ~1.5 nm AuNP,[37] which helped in the approximation of the total number of GS-AuNPs in the sample and, ultimately, the ratio between insulin and GS-AuNPs. In our study, we found that the small surface area of <2 nm GS-AuNPs favorably limited the number of proteins that can be conjugated to the NP surface, allowing a 1:1 ratio to be readily achievable. Prior to the animal injections, the concentration of the protein insulin conjugated to the NPs was measured by using the Bradford protein assay, a method that was also used similarly to that in a recently published work.[38] Figure 1E shows that the purified insulin-conjugated GS-AuNPs solution contains roughly 4.3 ± 0.1 mg/mL of insulin, which further substantiates the conjugation of the protein on the NPs, whereas the unconjugated GS-AuNPs essentially contain no protein.

Further characterization of the insulin-GS-AuNPs, as well as serum protein binding studies, was conducted using agarose gel electrophoresis. As shown in Figure 2A, the plain GS-AuNPs were found to progress faster than the insulin-GS-AuNPs, suggesting that the incorporation of the protein caused a significant increase in the overall mass/charge ratio of the conjugate and decrease in the electrophoretic mobility. The zeta potential (ζ) of the NPs was measured to determine their surface charge. As shown in Figure 2B, the pure GS-AuNPs have an overall charge of about −40 mV at pH 7.4, whereas the insulin-GS-AuNPs have roughly −10 mV, which is less negative due to the conjugation of insulin (ζ ~ −15 mV) and consistent with previous results.[39] Thus, the change in the NPs' overall surface charge, as well as their HD, correlates strongly with the gel electrophoresis results and further validates the attachment of insulin to the NPs. In addition, the serum protein binding was assessed by incubating the NPs with 10% fetal bovine serum (FBS) in phosphate buffered

saline (PBS) for 30 min at 37 °C and then were analyzed by agarose gel electrophoresis. Figure 2C shows that the insulin-GS-AuNPs incubated with FBS (2) have almost identical mobility as the insulin-GS-AuNPs without the FBS (1), based on their fluorescence (FL), but few NPs were observed to interact with serum proteins. On the other hand, the bright field (BF) image shows the binding of Coomassie brilliant blue 250 (CBB250) dye to the serum proteins (2′), also indicating low serum protein interaction, while the blue band for the serum-free insulin-GS-AuNPs (1′) is well separated. Understanding how these NPs interact with serum proteins in vitro can certainly help in determining their fate in vivo.[26]

The bioactivity of the insulin-GS-AuNPs was also assessed in vivo to determine whether the proteins are still capable of reducing the BGL. Using normal balb/c mice as a preliminary model, the ability of insulin-GS-AuNPs to lower blood glucose through specific binding to the insulin receptors can be evaluated and compared with free insulin. After the i.v. injection of the insulin-GS-AuNPs, the BGL of the balb/c mice was monitored for 6 h. As shown in Figure 2D, the BGL of the mice dropped to ~18% from its initial value during the first 2 h, which is similar to that of the free insulin (positive control). After 2 h, the BGL slowly reverted back above 20%, which is also comparable to that of free insulin. As a negative control, the pure GS-AuNPs and PBS were also i.v. injected to normal balb/c mice, and the BGL for both independent injections dropped to ~70% within the first 30 min post injection (p.i.) because of blood dilution, as shown in the same figure. Furthermore, the bioactivity of insulin-GS-AuNPs was also compared with that of dye-labeled insulin (Cy5.5-insulin) in the same experimental conditions. As shown in Figure S3A of the SI, the BGL of the normal balb/c mice also dropped to approximately 18% during the first 2 h, which is consistent with those of the free insulin and insulin-GS-AuNPs. Thus, these results clearly indicated that insulin can still target the insulin receptors and retain its bioactivity after being conjugated with the NPs.[40]

We examined how these NPs behaved and functioned in an actual diabetic mouse model. The same volume of insulin-GS-AuNPs solution (10 IU/kg) was i.v. injected to non-obese diabetic (NOD/ShiLtJ) mice that were fasted under the same conditions (4 h), and their BGL was monitored for 10 h. As shown in Figure 2E, the BGL decreased to ~21% within 2 h reaching the normal nondiabetic range, which is slightly lower than that of the free insulin (BGL: ~28%). As a negative control, the pure unconjugated GS-AuNPs were also used and i.v. injected for comparison. The BGL of the diabetic mice also decreased initially within the first half hour, because the blood was diluted by the administered sample. Although it was still in the diabetic range, the BGL swiftly escalated back up to near the original level as shown in Figure S3B in the SI. Unlike the normal balb/c mice, the NOD mouse model has an autoimmune disease that results in the pancreatic destruction of their insulin-generating β cells, which explains why their BGL immediately reverted.[41] Nevertheless, the insulin conjugated with the GS-AuNPs proves to be biologically active in the physiological environment, because it can target the insulin receptors that enable the protein to implement its function.

While renal-clearable GS-AuNPs have very low accumulation in different organs,[27,30] the conjugation of insulin induced significant change in the tissue biodistribution of the GS-AuNPs. As presented in Figure 3A, the insulin-GS-AuNPs had higher accumulation in the

organs such as kidneys (14.1%ID/g), liver (6.3%ID/g), and spleen (8.7%ID/g), which are nearly 2, 3, and 8 times higher than those of pure GS-AuNPs (kidneys 7.7%ID/g, liver 2.2%ID/g, spleen 1.1%ID/g), respectively. To reveal whether such an increase in the NP accumulation in these organs was due to the binding of the conjugated NPs to the insulin receptors, the ratio between the %ID/g obtained from the conjugated and unconjugated GS-AuNPs was calculated. As shown in Figure 3B, such an increase in the NP accumulation in the organs such as the liver and spleen, in particular, cannot be simply attributed to the increase of the overall HDs. For instance, it has been reported that the accumulation of nonluminescent GS-AuNPs with HD ~ 6 nm is nearly 30%ID/g and 12%ID/g in the liver and spleen, respectively.[27] Thus, the observed increases in the liver and spleen are more likely due to the interaction between the insulin and its receptor. Previous reports have shown that the insulin receptors are mainly distributed in the liver and spleen at a ratio of 0.71,[42] which is quantitatively consistent with our observation of the liver/spleen ratio (~0.72) of insulin-GS-AuNPs. This result is consistent with our bioactivity data that shows that insulin remains functional and can target the receptors after conjugation with renal-clearable GS-AuNPs. In addition, the NIR emission from GS-AuNPs also allowed us to monitor the renal clearance of untargeted insulin-GS-AuNPs. As depicted in Figure 3C, the bladder was illuminated within 10 min p.i. due to the urinary elimination of the NIR emitting GS-AuNPs. Figure S5 shows a direct comparison of the renal clearance kinetics, where the nontargeted insulin-GS-AuNPs was cleared through the urinary system with a $t_{1/2}$ of 8.7 min, which is comparable to that of unconjugated GS-AuNPs ($t_{1/2}$ of 9.4 min). The combination of all these results shows that the change in distribution of GS-AuNPs after conjugation to insulin is mainly due to their binding to the receptors, while the untargeted insulin-GS-AuNPs resulted in rapid renal clearance.

CONCLUSION

In summary, by using insulin as a model, we investigated how renal-clearable GS-AuNPs affect protein function and in vivo behaviors. We were able to successfully label insulin with NIR-emitting GS-AuNPs at a 1:1 ratio and demonstrated the insulin-GS-AuNPs' biological activity in lowering the blood glucose of diabetic mice. The blood glucose study revealed that the insulin-GS-AuNPs and pure insulin had comparable effectiveness in both normal and diabetic mouse models through i.v. administration. In addition, the untargeted insulin-conjugated GS-AuNPs are still capable of renal clearance as monitored via real-time NIR-FL imaging. Furthermore, the increase in the accumulation of insulin-GS-AuNPs in the liver and spleen, compared to pure GS-AuNPs, is due to the abundance of insulin receptors in those organs, in addition to the increase in HD. This quantitative understanding of how protein–NP conjugation and NP size influences the functionality and in vivo distribution of proteins in the native physiological environment without being "shadowed" by nonspecific serum protein adsorption will help more accurately control the in vivo behaviors of inorganic NPs and catalyze their biomedical applications.

EXPERIMENTAL PROCEDURES

Synthesis and Conjugation of NIR-Emitting GS-AuNPs with Insulin.

The NIR-emitting AuNPs were synthesized via a thermal reduction method.[14b,21] Briefly, 50 mL of 2.4 mM GSH solution was mixed with 150 μL 1 M $HAuCl_4 \cdot 3H_2O$ under vigorous stirring. The mixture was then heated in a 95 °C oil bath for ~30 min or until the fluorescence emission intensity (λ = 810 nm) of the solution reached the maximum monitored by a fluorescence spectrofluorometer. After the reaction, the resulting solution was cooled to room temperature. The pH of the sample was adjusted to ~2 using 1 M HCl and ~30 mL EtOH was added to precipitate out the NIR-emitting AuNPs. Then the sample was centrifuged at 4000 *g* for 5 min and the pellets were dispersed in 2 mL H_2O, followed by pH readjustment to neutral using 1 M NaOH. The sample solution was freeze-dried for 24–48 h. To conjugate insulin with the NIR-emitting AuNPs (GS-AuNPs), 12 mg and 16 mg of the EDC and NHS were dissolved, respectively, in 2 mL of the dried powder suspended in MES buffer (5 mg/mL GS-AuNPs) and allowd to react for 15 min. Afterwards, the solution was passed through a NAP25 column (washed with PBS) once to replace the buffer with pH 7.4. Meanwhile, 10 mg of human insulin was dissolved in 1 mL H_2O and the pH was adjusted to ~2, where the solubility of the protein is at its maximum. Then 3 mL of PBS was added into the insulin solution to adjust the pH to ~7.4. All of this was added to the 2 mL EDC-NHS reacted GS-AuNP solution. The mixture was left to react undisturbed for 2 h. After the 2 h reaction period, 135 mg glycine was added to the mixture to stop the reaction. The mixture was passed through a NAP25 column. Then, the insulin-conjugated AuNP solution was purified thoroughly by adjusting the pH to ~5.5 to precipitate out the insulin-conjugated AuNPs (Insulin-GS-AuNPs) and free insulin, leaving the unconjugated GS-AuNPs in the supernatant after centrifugation at 2000 *g* × 1 min. The pellets were dispersed in H_2O and the pH was readjusted back to neutral by the addition of 1 M NaOH. This procedure was performed 2 to 3 more times. Then, the pH of the sample was adjusted to ~2 to precipitate out the Insulin-GS-AuNPs (isoelectric point of the AuNPs), leaving the free insulin in the supernatant after centrifugation at 2000 *g* × 1 min. This was done 6 to 8 more times, followed by purification via NAP25 column. The final solution was centrifuged using Amicon Ultra 50 kDa centrifugal filter units to completely remove free insulin from the solution and the concentrate containing the Insulin-GS-AuNPs was diluted in a desired solvent (H_2O or PBS). The sample was kept at 4 °C until further study.

Bradford Protein Assay.

The estimated concentration of insulin in the Insulin-GS-AuNP sample was determined via Bradford Protein assay. The experimental protocol provided in the kit was conducted, but using insulin as the standard protein instead of Bovine Serum Albumin (BSA). Briefly, insulin standards were prepared with concentrations ranging from 0 to 750 μg/mL in H_2O. Then, 30 μL of a standard or sample was added to 1.5 mL of Coomassie Brilliant Blue (CBB) reagent solution and incubated for 10 min at room temperature. The absorbance of each of the standards and unknown samples were measured at 595 nm using a UV–vis spectrophotometer.

Enzyme Linked Immunosorbent Assay (ELISA).

The protocol provided in the insulin (human) ELISA kit was conducted without any modifications. Briefly, insulin standards, controls, and samples were added into the appropriate wells, the anti-insulin-HRP conjugate was added into these wells, and incubated for 30 min at room temperature. The liquid in the wells was discarded and washed 3 times with the wash buffer, followed by the addition of chromogen solution within 15 min after the washing step. The plate was incubated for another 15 min at room temperature in the dark. Afterward, a stop solution was added into each well, which resulted in the change of color from blue to yellow. The absorbance was measured at 450 nm using a microplate reader.

Glucose Tolerance Tests.

The animal studies were performed according to the guidelines of the University of Texas System Institutional Animal Care and Use Committee. The female NOD/ShiLtJ mice were purchased from The Jackson Laboratory at 8 weeks old. All of the animals were housed in ventilated cages under standard environmental conditions (23 ± 1 °C, 50 ± 5% humidity, and a 12/12 h light/dark cycle) with free access to water and standard laboratory food. The mice became diabetic between 25 and 30 weeks of age. All mice were anesthetized using 1.5–3% isofluorane with oxygen flowing at 0.8 L/min about 5 min prior to intravenous (i.v.) injection and blood collection. The mice were fasted for 4 h prior to and remained fasted for the duration of the experiment, but were given water ad libitum. The blood glucose level of the mice was measured prior to injection. The NOD/ShiLtJ mice (n = 3) were i.v. injected with 300 μL insulin-conjugated AuNPs (10 IU/kg) via tail vein and blood was collected via tail prick blood sampling at 0 min, 30 min, 1 h, 3 h, 6 h, and 10 h p.i. The blood glucose concentrations were determined by a glucose meter (One-Touch Ultra2).

Biodistribution of NIR-Emitting Insulin-Conjugated AuNPs.

Female Balb/c mice, strain code 555 (n = 3), 6–8 weeks old, weighing 20–25 g, were obtained from Charles River Laboratories. All mice were anesthetized using 1.5–3% isofluorane with oxygen flowing at 0.8 L/min about 5 min prior to intravenous (i.v.) injection. The mice were i.v. injected via tail vein with 300 μL Insulin-GS-AuNPs. After 2 h, the mice were sacrificed and their organs were collected for biodistribution. The collected organs were cut into small pieces, weighed, and completely lysed in 3 mL freshly made aqua regia in screw-capped glass scintillation vials (20 mL) separately for 24 h. The samples were then heated at 120 °C in an oil bath until the complete evaporation of aqua regia. The residue for each sample was then dispersed in 10 mL 0.05 M HCl, followed by sonication for 30–60 min, and centrifugation at 4000 g for 15 min. The resulting samples (supernatant) were then further diluted accordingly with 0.05 M HCl and the concentrations of gold (% injection dose/g, % ID/g) were determined using Agilent 7700x ICP Mass Spectrometer, a method similar to our previously published results.[19,30]

Fluorescence In Vivo Imaging.

The normal balb/c mice used for the in vivo fluorescence imaging studies were anesthetized using 1.5–3% isofluorane in oxygen flowing at 0.8 L/min about 5 min prior to the intravenous (i.v.) injection. Each mouse was preimaged before the i.v. injection. The

parameters used in the imaging for the Insulin-GS-AuNPs are described as follows: Insulin-GS-AuNPs (Excitation: 710 nm; Emission: 830 nm; Exposure time: 1 s). 300 μL of insulin-GS-AuNPs was injected intravenously in each balb/c mouse ($n = 3$), and the fluorescence (FL) was monitored by taking FL images of the mouse for 2 h.

Supplementary Material

Refer to Web version on PubMed Central for supplementary material.

ACKNOWLEDGMENTS

This manuscript was supported in part by the NIH (R01DK103363 and R21EB011762), CPRIT (RP120588 and RP140544), and the start-up fund from The University of Texas at Dallas (J.Z.). Special thanks to Prof. Xiankai Sun and Mr. Preston Christensen for the assistance with the ICP-MS measurements at UTSW, as well as to Ms Julia Dee Hankins of UTSW for helping with the ELISA studies.

REFERENCES

(1). Albanese A, Tang PS, and Chan WCW (2012) The Effect of Nanoparticle Size, Shape, and Surface Chemistry on Biological Systems. Annu. Rev. Biomed. Eng 14, 1–16. [PubMed: 22524388]

(2). Chan WCW, and Nie SM (1998) Quantum dot bioconjugates for ultrasensitive nonisotopic detection. Science 281, 2016–8. [PubMed: 9748158]

(3). Gao XH, Yang LL, Petros JA, Marshall FF, Simons JW, and Nie SM (2005) In vivo molecular and cellular imaging with quantum dots. Curr. Opin. Biotechnol 16, 63–72. [PubMed: 15722017]

(4). Huang X, Neretina S, and El-Sayed MA (2009) Gold Nanorods: From Synthesis and Properties to Biological and Biomedical Applications. Adv. Mater 21, 4880–910. [PubMed: 25378252]

(5). Huynh E, Leung BYC, Helfield BL, Shakiba M, Gandier J-A, Jin CS, Master ER, Wilson BC, Goertz DE, and Zheng G (2015) In situ conversion of porphyrin microbubbles to nanoparticles for multimodality imaging. Nat. Nanotechnol 10, 325–32. [PubMed: 25822929]

(6). Jin RC, Cao YC, Hao EC, Metraux GS, Schatz GC, and Mirkin CA (2003) Controlling anisotropic nanoparticle growth through plasmon excitation. Nature 425, 487–90. [PubMed: 14523440]

(7). Jones MR, Seeman NC, and Mirkin CA (2015) Programmable materials and the nature of the DNA bond. Science 347, 840.

(8). Ling D, Lee N, and Hyeon T (2015) Chemical Synthesis and Assembly of Uniformly Sized Iron Oxide Nanoparticles for Medical Applications. Acc. Chem. Res 48, 1276–85. [PubMed: 25922976]

(9). Rana S, Singla AK, Bajaj A, Elci G, Miranda OR, Mout R, Yan B, Jirik FR, and Rotello VM (2012) Array-Based Sensing of Metastatic Cells and Tissues Using Nanoparticle-Fluorescent Protein Conjugates. ACS Nano 6, 8233–40. [PubMed: 22920837]

(10). Choi HS, Gibbs SL, Lee JH, Kim SH, Ashitate Y, Liu F, Hyun H, Park G, Xie Y, Bae S, et al. (2013) Targeted zwitterionic near-infrared fluorophores for improved optical imaging. Nat. Biotechnol 31, 148–53. [PubMed: 23292608]

(11). Conway A, Vazin T, Spelke DP, Rode NA, Healy KE, Kane RS, and Schaffer DV (2013) Multivalent ligands control stem cell behaviour in vitro and in vivo. Nat. Nanotechnol 8, 831–38. [PubMed: 24141540]

(12). Howarth M, Liu W, Puthenveetil S, Zheng Y, Marshall LF, Schmidt MM, Wittrup KD, Bawendi MG, and Ting AY (2008) Monovalent, reduced-size quantum dots for imaging receptors on living cells. Nat. Methods 5, 397–9. [PubMed: 18425138]

(13). Cairo CW, Gestwicki JE, Kanai M, and Kiessling LL (2002) Control of Multivalent Interactions by Binding Epitope Density. J. Am. Chem. Soc 124, 1615–19. [PubMed: 11853434]

(14). Salvati A, Pitek AS, Monopoli MP, Prapainop K, Bombelli FB, Hristov DR, Kelly PM, Aberg C, Mahon E, and Dawson KA (2013) Transferrin-functionalized nanoparticles lose their targeting

capabilities when a biomolecule corona adsorbs on the surface. Nat. Nanotechnol 8, 137–43. [PubMed: 23334168]

(15). Deal KA, Motekaitis RJ, Martell AE, and Welch MJ (1996) Evaluation of the Stability and Animal Biodistribution of Gadolinium(III) Benzylamine-Derivatized Diethylenetriaminepenta-acetic Acid. J. Med. Chem 39, 3096–106. [PubMed: 8759630]

(16). Wang J, Bai R, Yang R, Liu J, Tang J, Liu Y, Li J, Chai Z, and Chen C (2015) Size- and surface chemistry-dependent pharmacokinetics and tumor accumulation of engineered gold nanoparticles after intravenous administration. Metallomics 7, 516–24. [PubMed: 25671498]

(17). Chen H, Wang GD, Tang W, Todd T, Zhen Z, Tsang C, Hekmatyar K, Cowger T, Hubbard RB, Zhang W, et al. (2014) Gd-Encapsulated Carbonaceous Dots with Efficient Renal Clearance for Magnetic Resonance Imaging. Adv. Mater 26, 6761–66. [PubMed: 25178894]

(18). Soo Choi H, Lui W, Misra P, Tanaka E, Zimmer JP, Itty Ipe B, Bawendi MG, and Frangioni JV (2007) Renal clearance of quantum dots. Nat. Biotechnol 25, 1165–70. [PubMed: 17891134]

(19). Zhou C, Hao G, Thomas P, Liu J, Yu M, Sun S, Oz OK, Sun X, and Zheng J (2012) Near-Infrared Emitting Radioactive Gold Nanoparticles with Molecular Pharmacokinetics. Angew. Chem., Int. Ed 51, 10118–22.

(20). Bhattacharyya S, Khan JA, Curran GL, Robertson JD, Bhattacharya R, and Mukherjee P (2011) Efficient Delivery of Gold Nanoparticles by Dual Receptor Targeting. Adv. Mater 23, 5034–38. [PubMed: 21971980]

(21). Cobley CM, Chen J, Cho EC, Wang LV, and Xia Y (2011) Gold nanostructures: a class of multifunctional materials for biomedical applications. Chem. Soc. Rev 40, 44–56. [PubMed: 20818451]

(22). Dreaden EC, Alkilany AM, Huang X, Murphy CJ, and El-Sayed MA (2012) The golden age: gold nanoparticles for biomedicine. Chem. Soc. Rev 41, 2740–79. [PubMed: 22109657]

(23). Giljohann DA, Seferos DS, Daniel WL, Massich MD, Patel PC, and Mirkin CA (2010) Gold Nanoparticles for Biology and Medicine. Angew. Chem., Int. Ed 49, 3280–94.

(24). Jain PK, Huang X, El-Sayed IH, and El-Sayed MA (2008) Noble Metals on the Nanoscale: Optical and Photothermal Properties and Some Applications in Imaging, Sensing, Biology, and Medicine. Acc. Chem. Res 41, 1578–86. [PubMed: 18447366]

(25). Wang M, and Thanou M (2010) Targeting nanoparticles to cancer. Pharmacol. Res 62, 90–9. [PubMed: 20380880]

(26). Vinluan R, and Zheng J (2015) Serum Protein Adsorption and Excretion Pathways of Metal Nanoparticles. Nanomedicine (London, U. K.) 10, 2781–94.

(27). Zhou C, Long M, Qin Y, Sun X, and Zheng J (2011) Luminescent Gold Nanoparticles with Efficient Renal Clearance. Angew. Chem., Int. Ed 50, 3168–72.

(28). Liu J, Yu M, Ning X, Zhou C, Yang S, and Zheng J (2013) PEGylation and Zwitterionization: Pros and Cons in the Renal Clearance and Tumor Targeting of Near-IR-Emitting Gold Nanoparticles. Angew. Chem., Int. Ed 52, 12572–6.

(29). Tu X, Chen W, and Guo X (2011) Facile one-pot synthesis of near-infrared luminescent gold nanoparticles for sensing copper (II). Nanotechnology 22, 095701. [PubMed: 21258146]

(30). Liu J, Yu M, Zhou C, Yang S, Ning X, and Zheng J (2013) Passive Tumor Targeting of Renal-Clearable Luminescent Gold Nanoparticles: Long Tumor Retention and Fast Normal Tissue Clearance. J. Am. Chem. Soc. 135, 4978–81. [PubMed: 23506476]

(31). Mo R, Jiang T, Di J, Tai W, and Gu Z (2014) Emerging micro- and nanotechnology based synthetic approaches for insulin delivery. Chem. Soc. Rev. 43, 3595–629. [PubMed: 24626293]

(32). Hovgaard L, Jacobs H, Mazer NA, and Kim SW (1996) Stabilization of insulin by alkylmaltosides. A. Spectroscopic evaluation. Int. J. Pharm 132, 107–13.

(33). Joshi HM, Bhumkar DR, Joshi K, Pokharkar V, and Sastry M (2006) Gold Nanoparticles as Carriers for Efficient Transmucosal Insulin Delivery. Langmuir 22, 300–5. [PubMed: 16378435]

(34). Chanana M, Correa-Duarte MA, and Liz-Marzan L (2011) Insulin-Coated Gold Nanoparticles: A Plasmonic Device for Studying Metal-Protein Interactions. Small 7, 2650–60. [PubMed: 21913324]

(35). Liu CL, Wu HT, Hsiao YH, Lai CW, Shih CW, Peng YK, Tang KC, Chang HW, Chien YC, Hsiao JK, et al. (2011) Insulin-Directed Synthesis of Fluorescent Gold Nanoclusters: Preservation of Insulin Bioactivity and Versatility in Cell Imaging. Angew. Chem., Int. Ed 50, 7056–60.

(36). Sarmento B, Ribeiro A, Veiga F, and Ferreira D (2006) Development and characterization of new insulin containing polysaccharide nanoparticles. Colloids Surf., B 53, 193–202.

(37). Azubel M, Koivisto J, Malola S, Bushnell D, Hura GL, Koh AL, Tsunoyama H, Tsukuda T, Pettersson M, Häkkinen H, et al. (2014) Electron microscopy of gold nanoparticles at atomic resolution. Science 345, 909–12. [PubMed: 25146285]

(38). Vinluan RD, Liu J, Zhou C, Yu M, Yang S, Kumar A, Sun S, Dean A, Sun X, and Zheng J (2014) Glutathione-Coated Luminescent Gold Nanoparticles: A Surface Ligand for Minimizing Serum Protein Adsorption. ACS Appl Mater. Interfaces 6, 11829–33. [PubMed: 25029478]

(39). Shimkunas RA, Robinson E, Lam R, Lu S, Xu X, Zhang X-Q, Huang H, Osawa E, and Ho D (2009) Nanodiamond–insulin complexes as pH-dependent protein delivery vehicles. Biomaterials 30, 5720–8. [PubMed: 19635632]

(40). Lee JP, and Paul F (1994) The insulin receptor: structure, function, and signaling. American Physiology Society, C319–34.

(41). Anderson MS, and Bluestone JA (2005) THE NOD MOUSE: A Model of Immune Dysregulation. Annu. Rev. Immunol 23, 447–85. [PubMed: 15771578]

(42). Jalilian AR, Garousi J, Akhlaghi M, and Rowshanfarzad P (2009) Development of ^{111}In labeled insulin for receptor imaging/therapy. J. Radioanal. Nucl. Chem 279, 791–6.

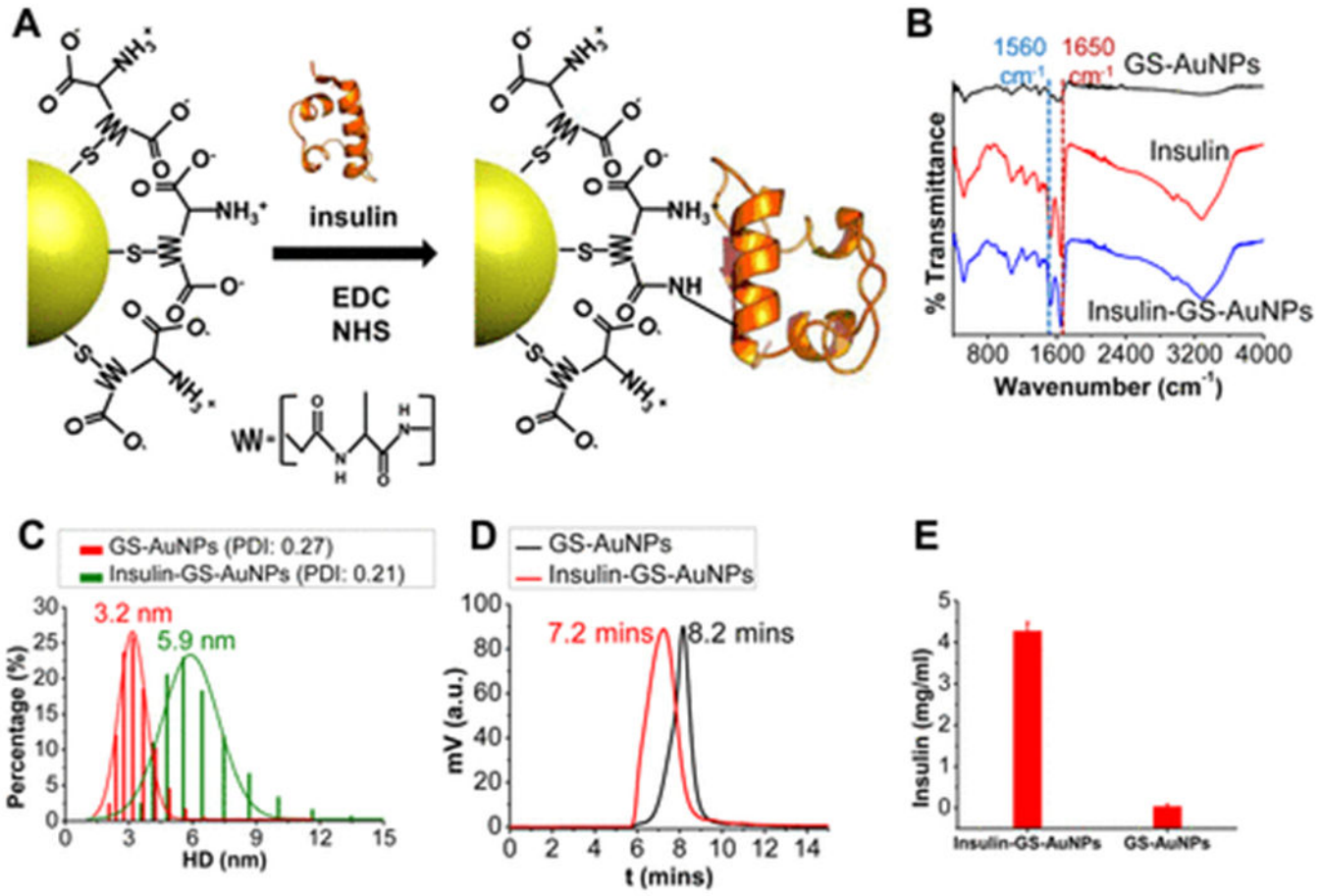

Figure 1.

Schematic diagram illustrating how the EDC-NHS coupling reaction was used to conjugate GS-AuNPs with insulin (A). IR spectra of GS-AuNPs compared to those of pure insulin and insulin-conjugated GS-AuNPs (B). HD and polydispersity index (PDI) of the NPs in PBS before and after conjugation (C). HPLC data for pure GS-AuNPs and insulin-GS-AuNPs (D). The concentration of insulin as determined via Bradford protein assay (E).

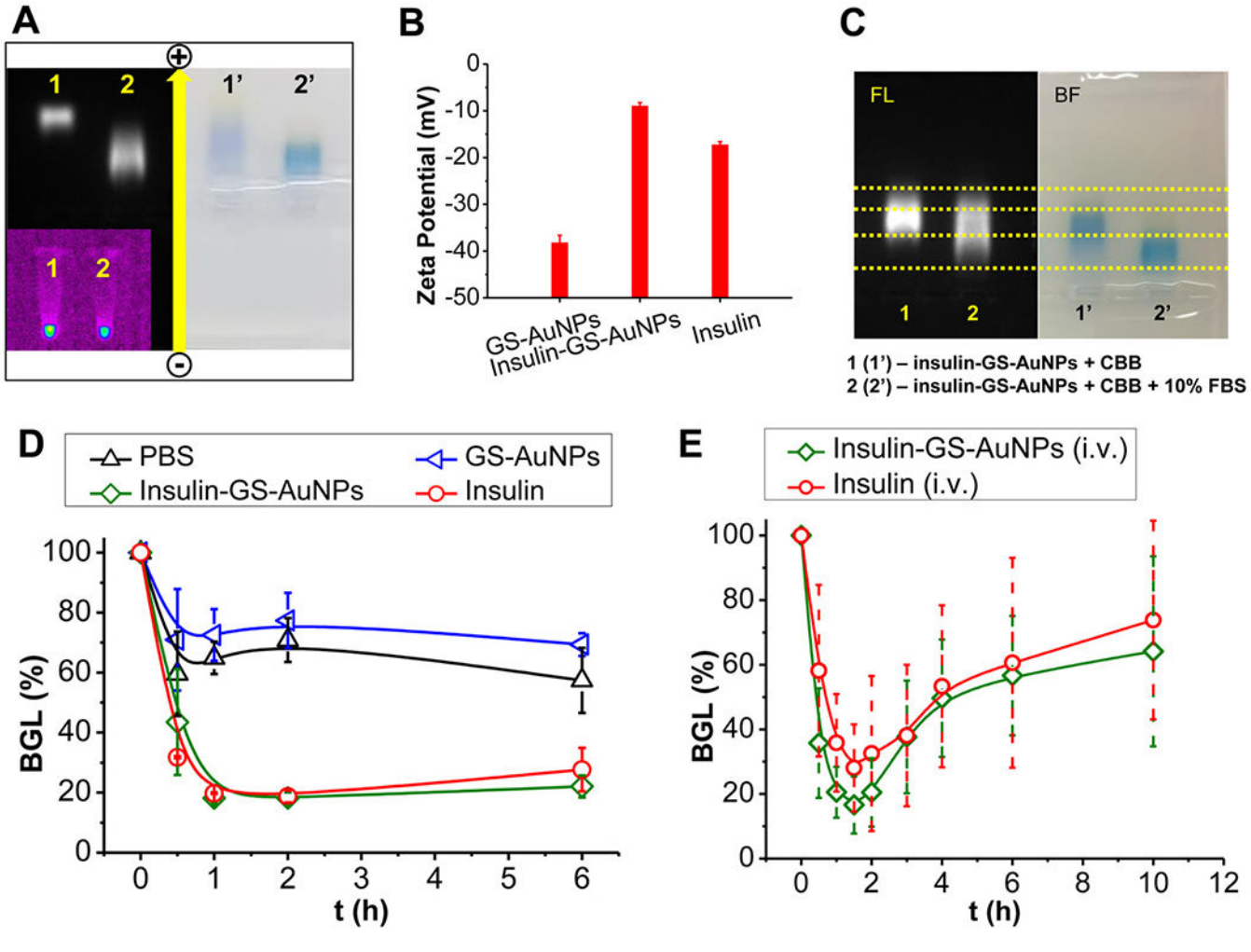

Figure 2.

Agarose gel electrophoresis showing the difference in electrophoretic mobility between the conjugated- (2) and unconjugated-GS-AuNPs (1) under FL field (left) and bright field (right) (A). Zeta potential charge comparison among pure GS-AuNPs, insulin, and insulin-GS-AuNPs (B). Serum protein binding analyzed via agarose gel electrophoresis (C). Bioactivity of the NPs was assessed using normal balb/c mice, and compared with positive and negative controls (D). NPs were also i.v. injected into diabetic mice (NOD/ShiLtJ) and the BGL was monitored for 10 h p.i., including the preinjection (E).

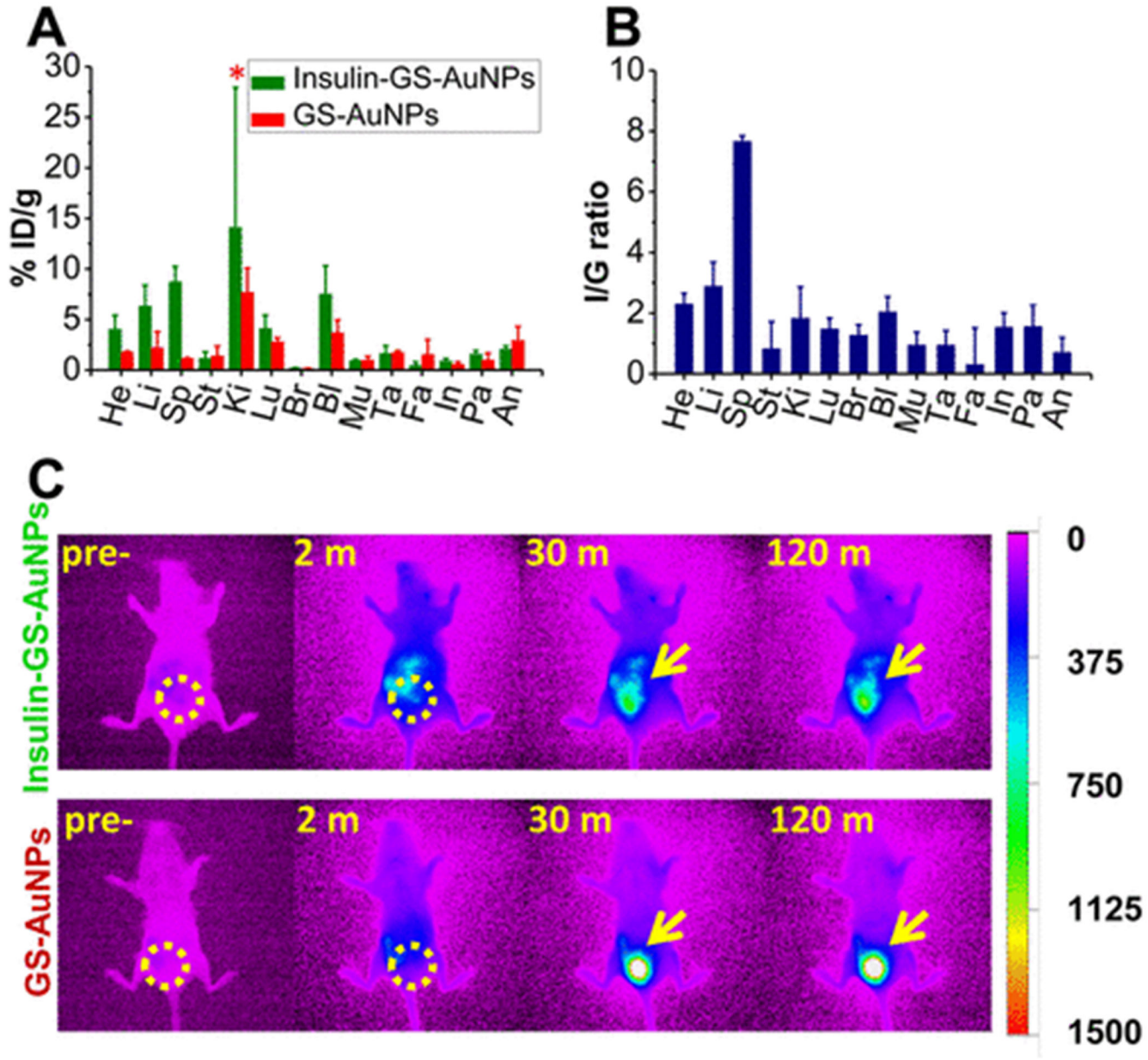

Figure 3.

Two hour biodistribution of insulin-GS-AuNPs compared to pure GS-AuNPs (A). The asterisk (*) indicates that a *t* test failed to reveal a statistically reliable difference between the two means ($p(0.237) > 0.05$). Ratio (*I/G*) between the %ID/g of Insulin-GS-AuNPs and %ID/g of GS-AuNPs (B). In vivo NIR FL imaging of normal balb/c mice after i.v. injection of GS-AuNPs (bottom) and insulin-GS-AuNPs (top) at 0, 2, 30, and 120 min time points (C), where the bladder region is circled and also indicated by arrows (FL intensity scale bar is shown on the right). (He, heart; Li, liver; Sp, spleen; St, stomach; Ki, kidneys; Lu, lungs; Br, brain; Bl, blood; Mu, muscle; Ta, tail; Fa, fat; In, intestines; Pa, pancreas; An, anus).